2. Nasimuddin, Z.N. Chen and X. Qing, Asymmetric-circular shaped slotted microstrip antennas for circular polarization and RFID applications, IEEE Trans Antennas Propag 58 (2010), 3821–3828.
3. P.M. Izdebski, H. Rajagopalan, and R.S. Yahya, Conformal ingestible capsule antenna: a novel chandelier meandered design, IEEE Trans Antennas Propag 57 (2009), 900–9009.
4. B. Hegyi and J. Levendovszky, Enhancing the performance of medical implant communication systems through cooperative diversity, Int J Telemedicine Appl 2010 (2010), Article ID 920704, 10 pages.
5. R. Garg, P. Bhartia, I. Bahl, and A. Ittipboon, Microstrip antenna design handbook, Artech House, Norwood, MA, 2001.
6. S.D. Targonski and D.M. Pozar, Design of wideband circularly polarized aperture-coupled microstrip antennas, IEEE Trans Antennas Propag 41 (1993), 214–219.
7. P.C. Sharma and K.C. Gupta, Analysis and optimized design of single feed circularly polarized microstrip antennas, IEEE Trans Antennas Propag 31 (1983), 949–955.
8. I. Iwasaki, A circularly polarized small size microstrip antenna with cross slot, IEEE Trans Antennas Propag 44 (1996), 1399–1401.
9. J.S. Row and Y. Ai, Compact design of single-feed circularly polarized microstrip antenna, Electron Lett 40 (2004), 1093–1094.
10. K.L. Wong and Y.F. Lin, Circularly polarized microstrip antenna with a tuning stub, Electron Lett 34 (1998), 831–832.
11. H.M. Chen and K.L. Wong, On the circular polarization operation of annular-ring microstrip antennas, IEEE Trans Antennas Propag 47 (1999), 1289–1292.
12. Nasimuddin, X. Qing, and Z.N. Chen, Compact circularly polarized microstrip antenna for RFID handheld reader applications, Asia Pacific Microwave Conference, Singapore, (2009), 1950–1953.
13. Nasimuddin, X. Qing, and Z.N. Chen, Compact asymmetric-slit microstrip antennas for circular polarization, IEEE Trans Antennas Propag 59 (2011), 285–288.
14. Zeland Software Inc., IE3D version 14.0, Zeland Software Inc., Fremont, CA, 2007.

INTERNAL CELLULAR HANDSET ANTENNA WITH A CURVED METAL PATTERN FOR DECREASED NEAR-FIELD RADIATION

Kin-Lu Wong and Hsuan-Jui Chang
Department of Electrical Engineering, National Sun Yat-Sen University, Kaohsiung 804, Taiwan; Corresponding author: wongkl@ema.ee.nsysu.edu.tw

Received 19 October 2011

ABSTRACT: *Near-field radiation characteristics of an internal cellular handset antenna with a curved metal pattern are studied. The antenna's metal pattern comprises a simple strip monopole for the GSM1800/1900 operation. The strip monopole is smoothly curved to avoid right-angle or abrupt bendings such that smooth variations of the excited surface currents thereon can be obtained. In this case, it is expected that the antenna's near-field radiation can be decreased. When compared with a corresponding monopole antenna with one or more right-angle bendings, the obtained results show that the proposed antenna can have lower specific absorption rate values by at least 1.0 dB, which is mainly owing to the decreased near-field radiation. Detailed results are presented and discussed.* © 2012 Wiley Periodicals, Inc. Microwave Opt Technol Lett 54:1927–1932, 2012; View this article online at wileyonlinelibrary.com. DOI 10.1002/mop.26958

Key words: *mobile antennas; internal handset antennas; curved metal patterns; near-field radiation; specific absorption rate; hearing aid compatibility*

1. INTRODUCTION

It has been shown that the low-Q antenna such as the ultrawideband or wideband antenna can have decreased near-field radiation, compared to the high-Q antenna such as the narrow-band antenna [1]. The peak electric and magnetic near-field strengths of the low-Q antenna were shown to be lower than those of a high-Q antenna by at least 5 dBV/m and 4 dBA/m, respectively. The decreased near-field radiation was shown to be related to the slope discontinuity of the excited surface current distributions on the antenna. Hence, a fat dipole antenna which has a low-Q property and a smooth surface current distribution can lead to decreased near-field radiation [1], compared to a traditional half-wavelength wire dipole antenna that shows a relatively high-Q property. In addition, the obtained bandwidth of the fat dipole antenna is much wider than that of the wire dipole antenna. However, it is noted that the occupied volume of the fat dipole antenna, which is generally obtained by increasing the arm width of the dipole antenna, is much larger than that of the wire dipole antenna. This makes the technique of increasing the antenna size to achieve a low-Q property to result in decreased near-field radiation less attractive for internal mobile device antenna applications, mainly due to the very limited space available inside the mobile device.

In this article, we demonstrate that simply by using a smoothly curved metal pattern for an internal cellular handset antenna, which generally does not increase the occupied volume of the antenna, the obtained near-field radiation characteristics such as the specific absorption rate (SAR) can be decreased, compared to a corresponding antenna with a metal pattern having right-angle or abrupt bendings. Results for a simple strip monopole for the GSM1800/1900 operation in the cellular handset are presented and discussed. Related results obtained for corresponding strip monopoles with a right-angle bending or multiple bendings are shown for comparison. The reason for decreased near-field radiation is because the excited surface currents on the strip monopole with a curved bending will experience a smooth variation on the surface current trace on the metal pattern of the antenna. On the other hand, the excited surface currents on the corresponding strip monopoles with a right-angle bending or multiple bendings will experience relatively abrupt changes on the surface current trace of the antenna's metal pattern, which will result in strong near-field electric fields as explained from the expression of the electric field $\vec{E}$ of an antenna given by [1, 2]

$$\vec{E} = \frac{1}{j2\pi f \mu\varepsilon}\left[k^2\vec{A} + \nabla(\nabla \cdot \vec{A})\right], \tag{1}$$

$$\vec{A} = \mu \iiint \vec{J}\frac{e^{-jkR}}{4\pi R}\,dV, \tag{2}$$

in which f is the operating frequency, μ is the permeability, ε is the permittivity, k is the wave number, and $\vec{A}$ is the magnetic vector potential. In Eq. (1), the term $\nabla(\nabla \cdot \vec{A})$ dominates the near-field radiation of the antenna, whereas the term $k^2\vec{A}$ dominates the far-field radiation [1, 2]. From Eq. (2), it is known that the magnetic vector potential is generally proportional to the excited surface current of the antenna. Hence, from the property of the term $\nabla(\nabla \cdot \vec{A})$, it can be expected that the abrupt variations of the excited surface currents on the metal pattern of the antenna will cause sharp increase in the near-field radiation of the antenna. This behavior will lead to increased SAR values [3–8] for the handset with such an antenna embedded therein. To verify this expectation, near-field radiation characteristics of

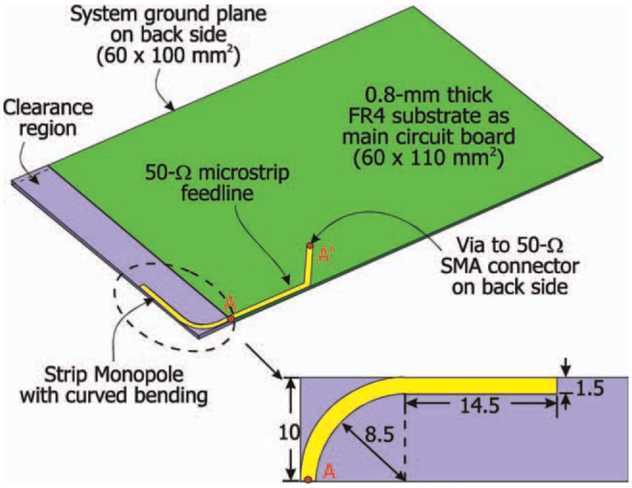

Figure 1 Geometry of the proposed internal cellular handset antenna with a curved metal pattern for the GSM1800/1900 operation. [Color figure can be viewed in the online issue, which is available at wileyonlinelibrary.com]

an internal cellular handset antenna with a curved metal pattern are studied, and obtained results are presented and discussed. The hearing aid compatibility (HAC) [9–12] results that are related to the near-field radiation of the antenna are analyzed as well.

2. STRIP MONOPOLES FOR THE GSM1800/1900 OPERATION

Figure 1 shows the geometry of the proposed internal cellular handset antenna with a curved metal pattern for the GSM1800/1900 operation. Corresponding internal GSM1800/1900 handset antennas with its metal pattern having a single bending (denoted as Ant1 in this study) or multibending (Ant2) are shown in Figure 2. The three antennas (proposed, Ant1, and Ant2) are strip monopoles with different bendings and can be seen more clearly from the photos of the fabricated prototypes shown in Figure 3. The three antennas are all printed on the clearance region ($10 \times$

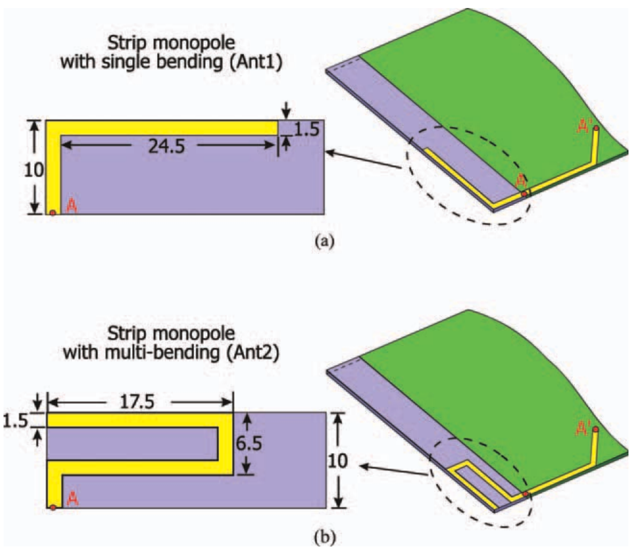

Figure 2 Geometries of the internal GSM1800/1900 handset antenna with its metal pattern having a single bending (Ant1) or multibending (Ant2). [Color figure can be viewed in the online issue, which is available at wileyonlinelibrary.com]

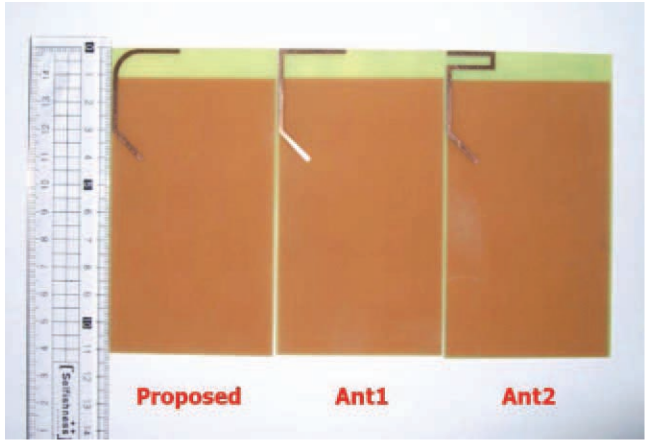

Figure 3 Photos of the fabricated prototypes of the proposed antenna, Ant1, and Ant2. [Color figure can be viewed in the online issue, which is available at wileyonlinelibrary.com]

60 mm^2) of the main circuit board of the handset, which is a 0.8-mm thick FR4 substrate of relative permittivity 4.4, loss tangent 0.024, and size 60×110 mm^2. On the back side of the main circuit board, a ground plane of size 60×100 mm^2 is printed. For feeding each strip monopole in the experiment, a 50-Ω microstrip feedline is printed on the front side of the main circuit board and is connected to a 50-Ω SMA connector at

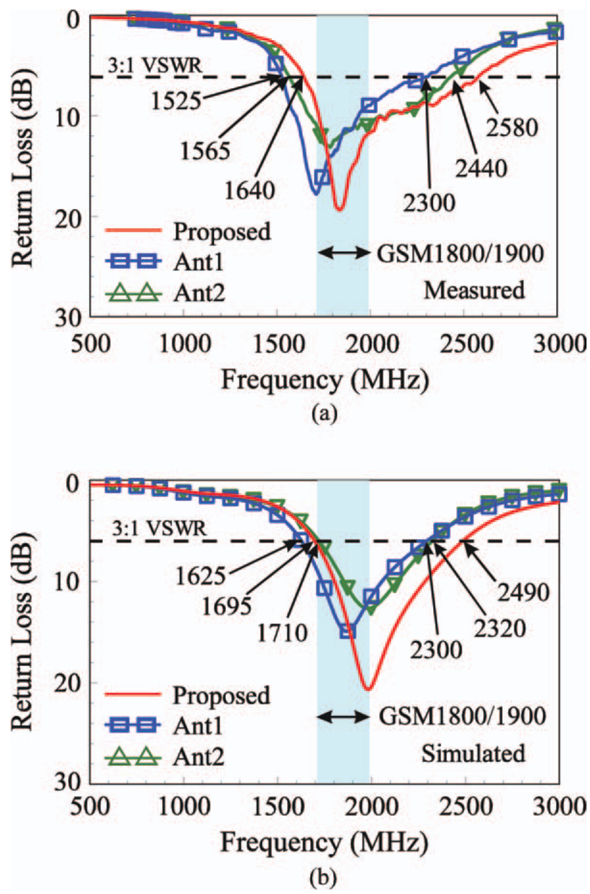

Figure 4 (a) Measured and (b) simulated return losses for the proposed antenna, Ant1, and Ant2. [Color figure can be viewed in the online issue, which is available at wileyonlinelibrary.com]

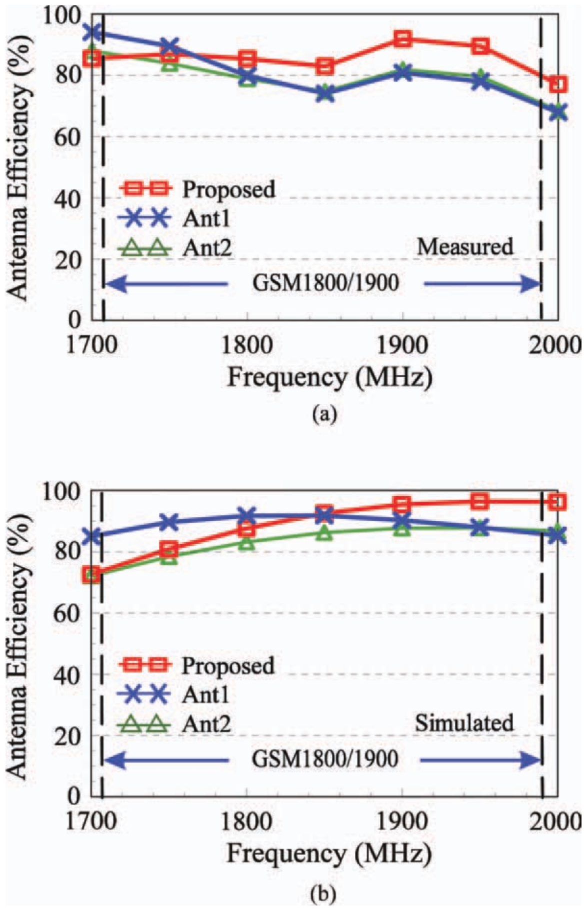

Figure 5 (a) Measured and (b) simulated antenna efficiencies (mismatching loss included) for the proposed antenna, Ant1, and Ant2. [Color figure can be viewed in the online issue, which is available at wileyonlinelibrary.com]

point A′ through a via-hole in the circuit board. The lengths of the three strip monopoles are adjusted such that the obtained bandwidths cover the GSM1800/1900 (1710–1880/1850–1990 MHz) bands in this study.

To confirm that the three antennas covered the desired operating bands, Figure 4 shows the measured and simulated return losses for the proposed antenna, Ant1, and Ant2. The simulated results are obtained using the SPEAG simulation software SEMCAD X version 14 [13] and generally agree with the measured data. Based on 3:1 VSWR or 6-dB return loss, which is widely used as the design specification of the internal handset antenna for the wireless wide area network operation [13–16], the operating bandwidths of the three antennas cover the GSM1800/1900 bands.

The measured and simulated antenna efficiencies that include the mismatching loss for the three antennas are also shown in Figure 5. The measured antenna efficiencies are generally in agreement with the simulated results. The small discrepancies between the measurement and simulation are mainly owing to the differences in the measured and simulated return losses seen in Figure 4. From the obtained results, it can be confirmed that the far-field radiation characteristics of the three antennas are about the same, and the obtained simulated results are also plausible as compared to the measured data. This can ensure good accuracy of the following simulation study on the near-field radiation characteristics of the three antennas.

3. NEAR-FIELD RADIATION OF THE STUDIED ANTENNAS

To analyze the near-field radiation characteristics, the SAR results are first studied. Figure 6 shows the SAR simulation models for three testing conditions of the head only, the hand only, and the head and hand. The SAR simulation models are based on the SPEAG SEMCAD X version 14 [17], and two cases of the antenna disposed at the top edge and bottom edge of the handset are studied. For each case, the handset with the antenna embedded therein is attached to the phantom head with no tilt. The distance between the ear and the system ground plane is 5 mm only, and that between the palm center and the system ground plane is 30 mm. The hand grip on the handset is shown in the figure.

The simulated SAR values for 1 g and 10 g tissues for the proposed antenna, Ant1, and Ant2, are presented in Figures 7 and 8, in which the results, respectively, for the antenna disposed at the top edge and bottom edge of the handset are presented. Results at representative frequencies of 1795 and 1920 MHz (center frequencies of the GSM1800 and GSM1900 bands) are shown. Figure 7 shows the results for the top-edge case. For fair comparison, the SAR results for the antennas with perfect matching condition (results with the # mark, part A and B in the figure) are also shown. For the head only condition, the 1 g and 10 g SAR values are the smallest for the proposed antenna, while those for Ant2 are the largest. For the hand only condition, the SAR values for Ant2 are also the largest. For the head and hand condition, the behavior is similar to that for the head

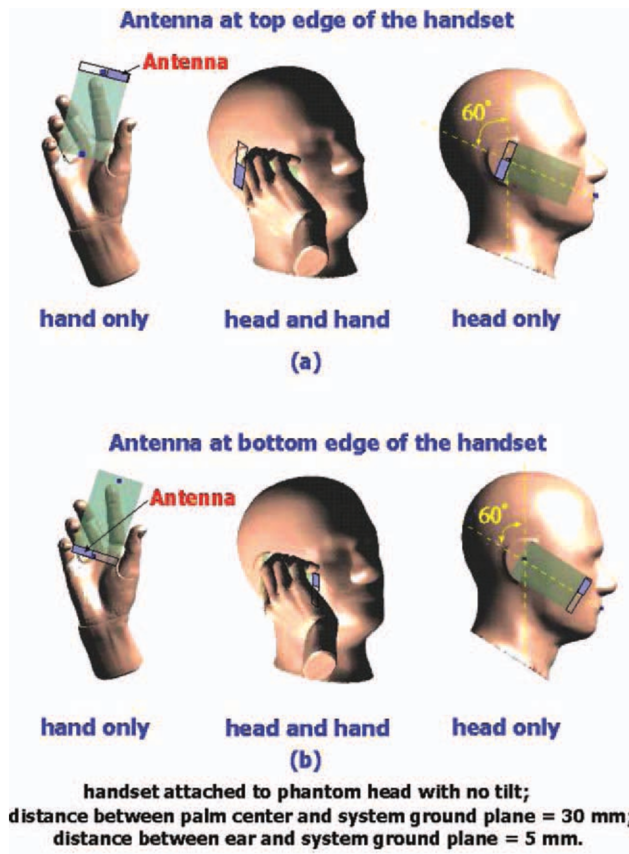

Figure 6 SAR simulation models for the head only, the hand only, and the head and hand conditions. (a) The antenna at top edge of the handset. (b) The antenna at bottom edge of the handset. [Color figure can be viewed in the online issue, which is available at wileyonlinelibrary.com]

Antenna at Top Edge of the Handset

Top edge		Proposed		Ant1		Ant2	
Frequency (MHz)		1795	1920	1795	1920	1795	1920
(A) 1-g SAR (W/kg)#	head only	1.63	1.57	1.67	1.64	1.78	1.77
	hand only	0.66	0.83	0.56	0.73	0.72	0.90
	head & hand	1.69 (1.69)	1.68 (1.67)	1.74 (1.73)	1.71 (1.70)	1.85 (1.82)	1.83 (1.81)
(B) 10-g SAR (W/kg)#	head only	0.92	0.90	1.02	1.00	1.08	1.07
	hand only	0.42	0.52	0.39	0.49	0.52	0.60
	head & hand	1.13 (0.95)	1.15 (0.95)	1.04 (1.04)	1.07 (1.04)	1.30 (1.10)	1.30 (1.10)
(C) 1-g SAR (W/kg)	head only	1.61	1.55	1.64	1.50	1.74	1.70
	hand only	0.60	0.82	0.54	0.70	0.62	0.85
	head & hand	1.67 (1.67)	1.64 (1.64)	1.69 (1.68)	1.55 (1.55)	1.80 (1.78)	1.75 (1.74)
(D) 10-g SAR (W/kg)	head only	0.89	0.89	1.00	0.92	1.04	1.01
	hand only	0.38	0.52	0.38	0.47	0.41	0.56
	head & hand	1.12 (1.01)	1.12 (0.98)	1.02 (1.02)	0.97 (0.94)	1.26 (1.06)	1.25 (1.04)
Return Loss (dB)	head only	20.7	18.3	16.9	10.7	15.4	13.4
	hand only	10.4	17.9	14.7	14.3	9.2	13.1
	head & hand	21.2	16.9	15.5	10.3	15.5	13.5
	free space	9.6	17.7	12.9	14.0	8.1	12.0

#: Considered under Perfect matching
( ): SAR value occurred at head for the head and hand condition

Figure 7 Simulated SAR values for 1 g and 10 g tissues for the proposed antenna, Ant1, and Ant2. The antenna is at the top edge of the handset. [Color figure can be viewed in the online issue, which is available at wileyonlinelibrary.com]

only condition, indicating that the head dominates the SAR behavior. Also note that the SAR values in the parentheses are occurred at head for the head and hand condition. When the values in the parentheses are smaller, it indicates that maximum power absorption in the head and hand condition is occurred at hand and not at head. For the SAR results for the antennas with the mismatching condition considered (part C and D in the figure), similar behavior as that observed for the perfect matching condition is seen. This also indicates that there are no large frequency shifts when the head and/or hand are in proximity to the three antennas in the study. This can also be seen from the return losses for the antennas in free space and three testing conditions shown in the figure. In general, in the top-edge case, it can be concluded that the antenna with multibending (Ant2) show increased SAR values, whereas the proposed antenna shows decreased SAR values. This observation is believed to be related to the near-field radiation characteristics of the antenna with smooth or abrupt bendings as discussed in Section 2.

Figure 8 shows the results for the bottom-edge case. Although the hand generally encloses the antenna in this case, the SAR values for the head and hand condition are seen to be much lower than those obtained in Figure 7 for the top-edge case. Again, the SAR values in part A and B are for the perfect matching condition, whereas those in part C and D are for the mismatching condition. The SAR values for both Ant1 and Ant2 are also observed to be about the same and larger than those of the proposed antenna by at least 1 dB (25% larger) for the 1 g tissue case (e.g., at 1795 MHz for the head only case in part A, 0.50 W/kg for the proposed antenna vs. 0.65 W/kg for Ant1 and Ant2). The decrease in the SAR values for the bottom-edge case is more significant than that observed in Figure 7 for the top-edge case. It is also seen that the obtained 1 g and 10 g SAR values are all less than the required limits (1.6 W/kg for 1 g tissue [3] and 2.0 W/kg for 10 g tissue [4]) for practical applications, with the proposed antenna having the lowest SAR values. This is also believed to be related to the near-field radiation characteristics of the antenna with smooth or abrupt bendings as discussed in Section 2. The obtained results indicate that, by using a smooth or curved metal pattern for the internal handset antenna, the obtained SAR results can have decreased values, especially when the antenna is disposed at the bottom edge of the handset.

The HAC results are also analyzed. Figure 9 shows the HAC simulation model with the antenna disposed at the bottom edge of the handset. The HAC simulation model is also based on the SPEAG SEMCAD X version 14 [17]. Figure 10 shows the simulated HAC results for the three antennas. In Figures 10(a) and 10(b), the HAC results of the cases with the perfect matching condition and the mismatching condition are, respectively, presented. Also note that in Figure 10(b), based on the rule of ANSI C63.19-2007 [8], the near-field E-field and H-field strengths at the HAC observation plane divided into nine cells above the acoustic output are determined by excluding three consecutive cells along the boundary of the observation plane

Antenna at Bottom Edge of the Handset

Bottom edge		Proposed		Ant1		Ant2	
Frequency (MHz)		1795	1920	1795	1920	1795	1920
(A) 1-g SAR (W/kg)#	head only	0.50	0.51	0.65	0.67	0.65	0.68
	hand only	0.73	0.68	1.10	1.06	0.99	1.10
	head & hand	0.58 (0.48)	0.68 (0.50)	1.03 (0.62)	1.07 (0.64)	0.97 (0.61)	1.18 (0.63)
(B) 10-g SAR (W/kg)#	head only	0.36	0.36	0.42	0.43	0.40	0.42
	hand only	0.32	0.40	0.58	0.59	0.54	0.62
	head & hand	0.35 (0.33)	0.46 (0.34)	0.61 (0.41)	0.72 (0.42)	0.57 (0.39)	0.69 (0.40)
(C) 1-g SAR (W/kg)	head only	0.40	0.47	0.60	0.67	0.59	0.65
	hand only	0.53	0.58	0.93	1.00	0.86	1.09
	head & hand	0.47 (0.38)	0.62 (0.45)	0.94 (0.57)	1.04 (0.63)	0.92 (0.58)	1.17 (0.63)
(D) 10-g SAR (W/kg)	head only	0.28	0.34	0.38	0.43	0.36	0.40
	hand only	0.23	0.34	0.50	0.56	0.47	0.59
	head & hand	0.28 (0.27)	0.41 (0.32)	0.55 (0.37)	0.70 (0.41)	0.54 (0.37)	0.69 (0.40)
Return Loss (dB)	head only	6.6	11.4	10.6	24.2	10.1	13.7
	hand only	5.5	8.3	8.2	13.2	9.2	14.0
	head & hand	7.0	10.4	10.6	15.7	12.9	21.1
	free space	9.6	17.7	12.9	14.0	8.1	12.0

#: Considered under Perfect matching
( ): SAR value occurred at head for the head and hand condition

Figure 8 Simulated SAR values for 1 g and 10 g head tissues for the proposed antenna, Ant1, and Ant2. The antenna is at the bottom edge of the handset. [Color figure can be viewed in the online issue, which is available at wileyonlinelibrary.com]

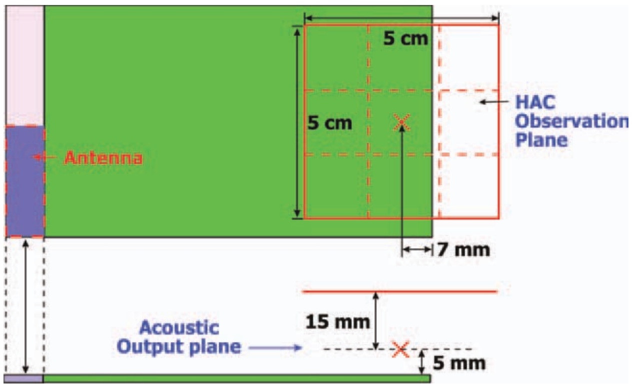

Figure 9 HAC simulation model with the antenna disposed at the bottom edge of the handset. [Color figure can be viewed in the online issue, which is available at wileyonlinelibrary.com]

that have the strongest field strengths. On the other hand, the results shown in Figure 10(a) are the strongest E-field and H-field strengths among all the nine cells of the HAC observation plane. From the obtained results, although the proposed antenna shows the smallest E-field and H-field strengths in both conditions shown in Figure 10, the decrease in the E-field and H-field strengths is small, compared to the field strengths of Ant1 and Ant2. The different effects on the SAR and HAC behavior are largely because the SAR values are determined by the power absorption in a small-volume tissue (1 g or 10 g tissue). Hence, although the field variations may be small in view of the HAC behavior, the SAR variations could be relatively much larger as observed in Figures 7 and 8.

4. CONCLUSIONS

The SAR and HAC results of the internal GSM1800/1900 handset antenna formed by a strip monopole with a curved bending, a right-angle bending, and multibendings have been studied. The antennas in the study are all with good impedance matching and good antenna efficiencies for frequencies over the GSM1800/1900 bands. That is, similar far-field radiation characteristics have been obtained. However, from the obtained SAR results, especially for the antenna disposed at the bottom edge of the handset, the proposed antenna with a smooth or curved metal pattern can have decreased SAR values by at least 1 dB, compared to those of the corresponding antennas with right-angle bendings. This behavior is believed to be related to the smooth variations of the excited surface currents on the curved metal pattern of the proposed antenna. For the HAC results, the proposed antenna with a smooth or curved metal pattern is still with decreased HAC values, although the decrease in the HAC values is much smaller than that in the SAR values. The difference in the obtained SAR and HAC results are largely because the SAR values are determined by the power absorption in a small-volume tissue (1 g or 10 g tissue), not like the HAC that is related to the field strength variation on the HAC observation plane. From the obtained results in this study, it can be concluded that simply by applying a smooth or curved metal pattern for the internal cellular handset antenna, it is very helpful to achieve decreased SAR values or decreased near-field radiation of the handset with the antenna embedded therein.

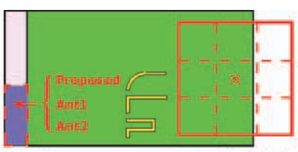

Perfect Matching Considered

Frequency (MHz)	1795	1920
E-field (dB, V/m) (Proposed)	42.7	42.1
E-field (dB, V/m) (Ant1)	42.7	42.1
E-field (dB, V/m) (Ant2)	43.0	42.5
H-field (dB, A/m) (Proposed)	-8.4	-9.0
H-field (dB, A/m) (Ant1)	-8.4	-9.0
H-field (dB, A/m) (Ant2)	-7.9	-8.5

(a)

Mismatching Considered

Frequency (MHz)	1795	1920
E-field (dB, V/m) (Proposed)	39.9	39.6
E-field (dB, V/m) (Ant1)	40.3	39.6
E-field (dB, V/m) (Ant2)	40.4	40.3
H-field (dB, A/m) (Proposed)	-10.6	-10.8
H-field (dB, A/m) (Ant1)	-10.4	-10.9
H-field (dB, A/m) (Ant2)	-10.5	-10.5

(b)

Figure 10 Simulated HAC results for the proposed antenna, Ant1, and Ant2 with the HAC model shown in Figure 9. (a) The case with perfect matching considered. (b) The case with mismatching and ANSI C63.19-2007 rules considered. [Color figure can be viewed in the online issue, which is available at wileyonlinelibrary.com]

REFERENCES

1. T. Yang, W.A. Davis, W.L. Stutzman, and M.C. Huynh, Cellular-phone and hearing-aid interaction: An antenna solution, IEEE Antennas Propag Mag 50 (2008), 51–65.
2. W.L. Stutzman and G.A. Thiele, Antenna theory and design, 2nd ed., Wiley, New York, 1998.
3. American National Standards Institute (ANSI), Safety levels with respect to human exposure to radio frequency electromagnetic fields, 3 kHz to 300 GHz, ANSI/IEEE standard C95.1, 1999.
4. IEC 62209-1, Human exposure to radio frequency fields from hand-held and body-mounted wireless communication devices—Human models, instrumentation, and procedures—Part 1: Procedure to determine the specific absorption rate (SAR) for hand-held devices used in close proximity to the ear (frequency range of 300 MHz to 3 GHz), 2005.
5. K.L. Wong and W.J. Lin, Body SAR study of the planar WWAN monopole slot antenna for tablet device application, Microwave Opt Technol Lett 53 (2011), 1721–1727.
6. K.L. Wong, W.J. Wei, and L.C. Chou, WWAN/LTE printed loop antenna for tablet computer and its body SAR analysis, Microwave Opt Technol Lett 53 (2011), 2912–1919.
7. Y.W. Chi and K.L. Wong, Compact multiband folded loop chip antenna for small-size mobile phone, IEEE Trans Antennas Propag 56 (2008), 3797–3803.
8. American National Standard for Method of Measurement of Compatibility between Wireless Communication Devices and Hearing Aids (ANSI C63.19-2007), American National Standards Institute, New York, 2007.
9. K.L. Wong and M.F. Tu, Hearing aid-compatible internal penta-band antenna for clamshell mobile phone, Microwave Opt Technol Lett 51 (2009), 1408–1413.
10. W.Y. Li and K.L. Wong, Small-size WWAN loop chip antenna for clamshell mobile phone with hearing-aid compatibility, Microwave Opt Technol Lett 51 (2009), 2327–2335.
11. W.Y. Chen and K.L. Wong, Wideband coupled-fed PIFA for HAC penta-band clamshell mobile phone, Microwave Opt Technol Lett 51 (2009), 2369–2374.
12. S.C. Chen and K.L. Wong, Hearing aid-compatible internal LTE/WWAN bar-type mobile phone antenna, Microwave Opt Technol Lett 53 (2011), 774–781.
13. C.L. Liu, Y.F. Lin, C.M. Liang, S.C. Pan, and H.M. Chen, Miniature internal penta-band monopole antenna for mobile phones, IEEE Trans Antennas Propag 58 (2010), 1008–1011.
14. W.S. Chen and S.H. Din, A novel printed monopole antenna for GSM/DCS/PCS/UMTS band operation, Microwave Opt Technol Lett 51 (2009), 2453–2458.

15. K.L. Wong, W.Y. Chen, and T.W. Kang, On-board printed coupled-fed loop antenna in close proximity to the surrounding ground plane for penta-band WWAN mobile phone, IEEE Trans Antennas Propag 59 (2011), 751–757.
16. K.L. Wong and S.C. Chen, Printed single-strip monopole using a chip inductor for penta-band WWAN operation in the mobile phone, IEEE Trans Antennas Propag 58 (2010), 1011–1014.
17. SPEAG SEMCAD, Schmid & Partner Engineering AG, Available at: http://www.semcad.com.

ESTIMATION OF COUPLING PARAMETERS FOR AUTO-MOTORIZED FABRICATION OF FUSED FIBER COUPLER

Dedi Irawan,[1] Saktioto,[1,2] Jalil Ali,[2] Mohamed Fadhali,[3] and Erwin [1]
[1] Faculty of Science, APSI, Universiti Teknologi Malaysia, Johore, Malaysia 81310; Corresponding author: dedi.dawan@yahoo.com
[2] Faculty of Math and Sciences, Department of Physics, University of Riau, Pekanbaru, Indonesia
[3] Faculty of Science, Department of Physics, Ibb University, Ibb, Yemen

Received 27 October 2011

ABSTRACT: *A directional fiber coupler with exertion loss 0.03 dB has been successfully fabricated using fusion technique with typical coupling ratio 1–90%. The coupling region of two twisted single mode fiber is heated by injecting hydrogen gas at 2.5 bar. During fusion process, both two sides of fibers are pulled by stages that are automatically motorized in range of 800–4800 μm, and stopped when the desired coupling ratio is reached. The parameters of automated mechanical motion of pulling stages and coupling parameters at fusion region have been calculated by using kinetic model. The effect of heating and elongation reduces the diameter of cross section tapered region with a diameter 6.35 micrometer scale. As the fabrication of fiber couplers described by degree of fusion, which is function of heating and pulling length, it can be seen clearly that the coupling coefficient between the fibers increases exponentially with increasing the degree of fusion. However, by knowing coupling power and mechanical motion parameters, the fabrication of directional fiber coupler can be optimized.* © 2012 Wiley Periodicals, Inc. Microwave Opt Technol Lett 54:1932–1935, 2012; View this article online at wileyonlinelibrary.com. DOI 10.1002/mop.26937

Key words: *directional fiber coupler; pulling length; degree of fusion; coupling ratio; coupling coefficient*

1. INTRODUCTION

The use of optical devices on network communication system has been widely expanded. It provides an optical circuit that can carry out data in terms of audio, video, data processing, etc. with big capacity, low loss, and faster. Optical directional fiber coupler is a passive device and main component of optical networking system. It is used to split, to combine, or to switch optical signal. As the networking system is built by using optical components, a directional fiber coupler with various coupling ratio is always needed. The fiber coupler can be fabricated by using twist-etching techniques, polishing technique, and fusion technique [1, 2].

Fusion and elongation is an easier technique that has been used to fabricate fiber coupler. In 2005, Fused bi-conical tapered (FBT) coupler was fabricated by this technique. The coupling region was heated by CO_2 laser, and resulting good FBT couplers with 3-dB splitting ratio [3]. Because of CO_2 laser beam is a high cost technology, fusion technique by injecting H_2 gas to the torch flame was purposed for hearting the coupling region [4]. During fusion, fibers are elongated in micrometer scale until the coupling ratio is reached. Since that fabrication results high coupling loss, the study of the automated fiber coupler fabrication system based on fusion technique becomes necessary to determine coupling parameters [5–9].

In this article, the coupling parameters are estimated to optimize auto control parameters for fabrication of directional fiber coupler so that good performance of directional fiber coupler reached.

2. THEORETICAL CONSIDERATION

The propagation of an optical signal in the coupled waveguide medium was determined clearly from the Maxwell equation using coupling-mode theory method [5]. The modeling and experiment of power parameters SMF coupler were also studied [6]. It showed the coupling ratio as the function of coupling coefficient between the fibers. As the refractive indices of coupled fibers are constant, and geometrical fibers are also identical as shown in Figure 1, the amplitude of power exchanges between two fibers given by Eq. (1).

$$\begin{bmatrix} P_a(z) \\ P_b(z) \end{bmatrix} = \begin{bmatrix} \cos\sigma z - \frac{j\delta}{\sigma}\sin\sigma z & -\frac{j\kappa_2}{\sigma}\sin\sigma z \\ -\frac{j\kappa_1}{\sigma}\sin\sigma z & \cos\sigma z - \frac{j\delta}{\sigma}\sin\sigma z \end{bmatrix} \begin{bmatrix} P_a(0) \\ P_b(0) \end{bmatrix} \quad (1)$$

where P_a and P_b are power amplitudes in fibers 1 and 2, respectively. The coupling coefficient is denoted by k, and L is coupling length. As the coupling region is tapered due to fusion and elongation, and by defining the degree of fusion f is a factor that describes how close two fibers joined or $f = x/y$, a simple relationship between degree of fusion separation between fiber's core d can be written as follows:

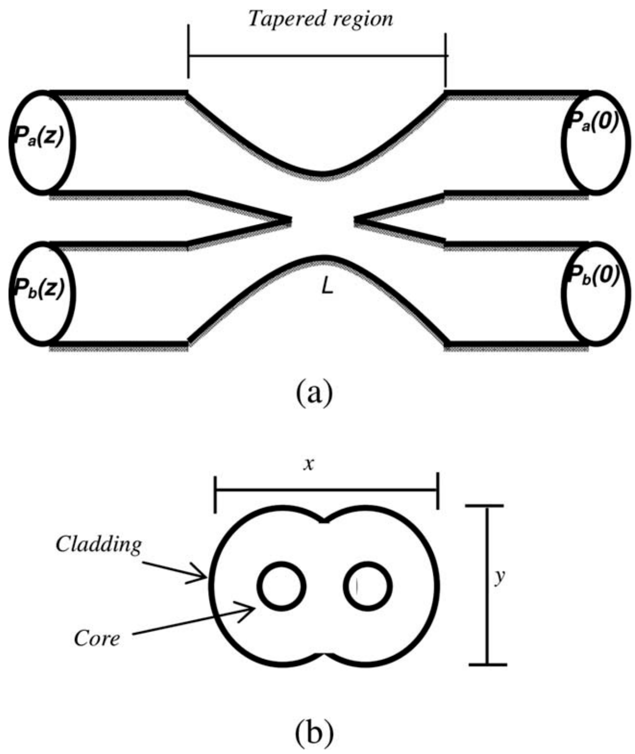

Figure 1 Illustration of geometrical fused fiber coupler, (a) tapered directional fiber coupler and (b) cross section of coupling region